Application Note

Magnet Selection for Linear Position Applications

ABSTRACT

For position-sensing applications such as linear motor transport systems that must detect the position of a magnet sliding along a linear path, the geometry of the magnet and the relative air gap to the sensor influences the behavior of the magnetic field as the magnet passes by the sensor.

Additionally, in any system the sensing range must be maximized for each sensor to reduce component count and save cost. In smaller applications that require only a low quantity of sensors, often the cost of the single magnet can overwhelm the total cost of the sensors. However, designers can consider the use of a slightly larger magnet to reduce the total number of sensors in large arrays.

This application note discusses the placement, calibration, and sensing range of various magnet geometries and materials with 3D magnetic sensors, like the TMAG5170 and TMAG5273, in linear arrays.

Table of Contents

List of Figures

List of Tables

Trademarks

All trademarks are the property of their respective owners.

1 Introduction

When detecting the linear motion of a magnet in any system, designers must maximize the total sensing range of the sensor for a particular magnet in use while maintaining a tight tolerance on overall measured position error. This strategy allows the designer to minimize the size of the magnet and reduce the total number of Hall-effect sensors needed in an array to capture the full stroke length of the system.

Tighter tolerances for magnetic position sensing produce improved feedback in controlled systems like linear motor transport systems by providing exact locations for each individual mover in the system. In linear motor transport systems, there are typically several individual movers that drive around a track or platform using repeating linear motors. For any mover, understanding absolute position at all times is important to properly place the target at each manufacturing step, to efficiently move the platforms for maximum throughput, and to accurately drive the motor stage controlling that position.

Traditionally, this function has been supported by one-dimensional linear Hall-effect sensors, such as the DRV5055 which capture the z-component of the magnetic field when using the SOT-23 package.

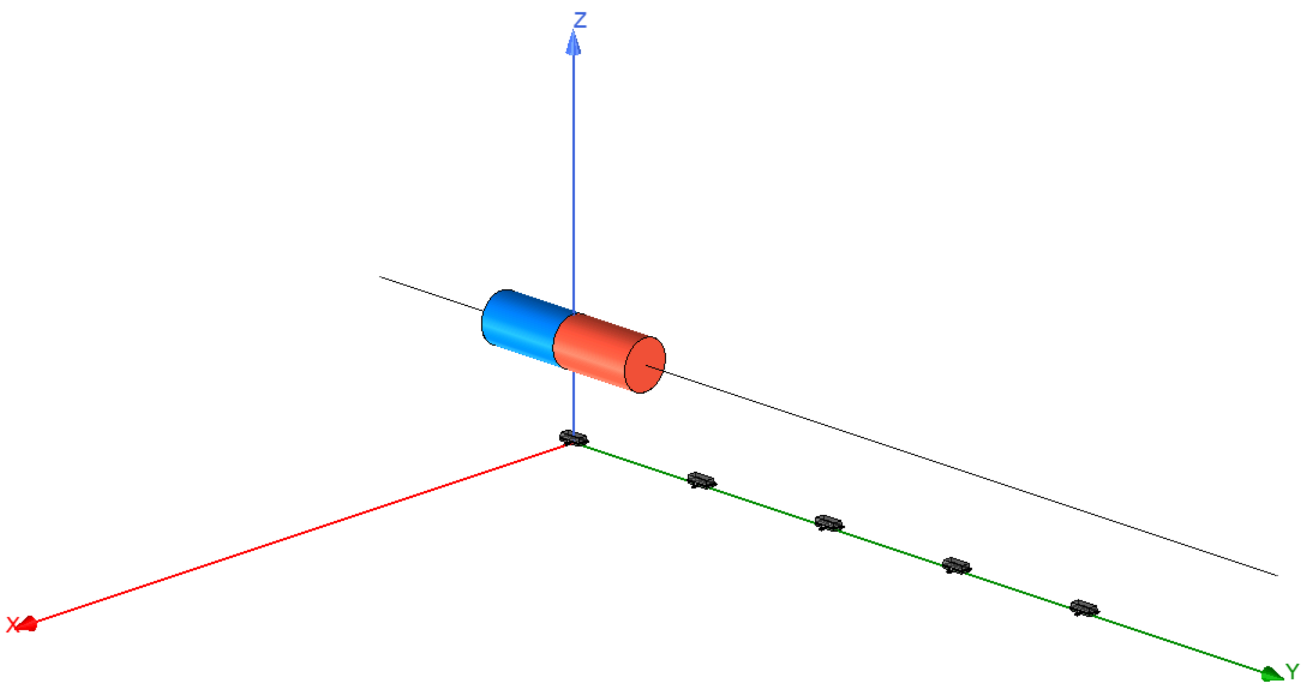

Figure 1-1. Linear Position Sense Array With One-Dimensional Hall-Effect Sensors

In this style of position-sensing configuration, the sensing range is limited to a linear region of the input magnetic field which is approximately the length of the magnet.

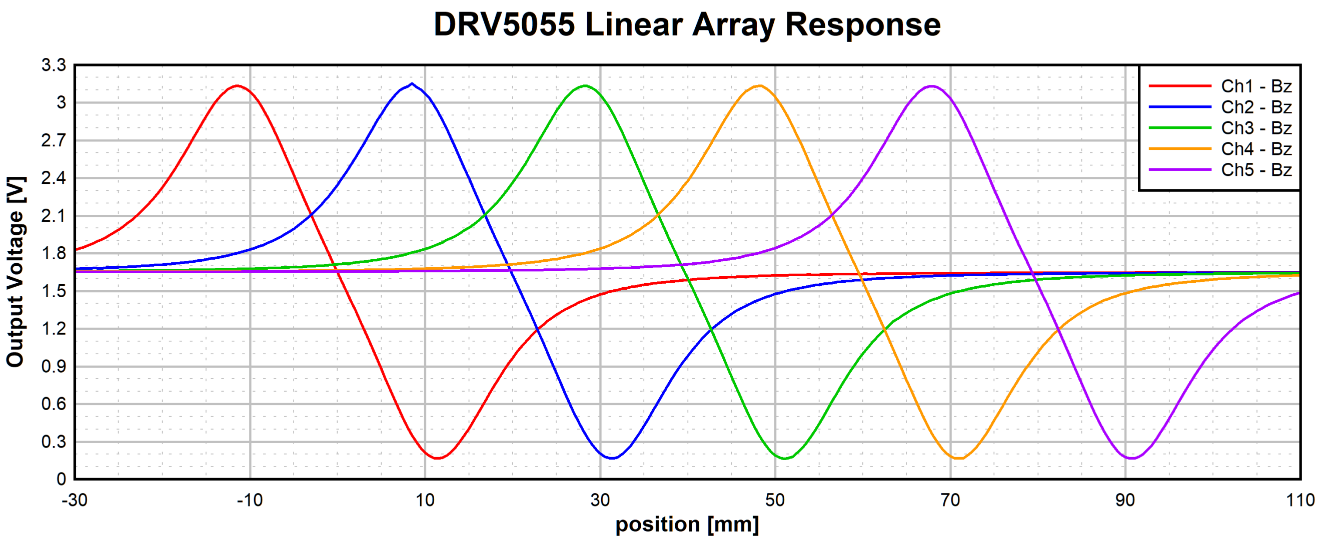

Figure 1-2. DRV5055 Output in Linear Array Configuration

This configuration is described in more detail in *Linear Hall Effect Sensor Array Design*, application note.

There are significant advantages gained by implementing this design using a 3D linear Hall-effect sensor like the TMAG5170 or TMAG5273. Firstly, the sensors are capable of detecting each component of the complete B-field vector. With expanded information, we can identify exact magnet position over a range of motion longer stroke lengths than can be detected using a single axis sensor. Additionally, these sensors have integrated functions for amplitude and offset correction which are useful for correcting various electro-mechanical factors.

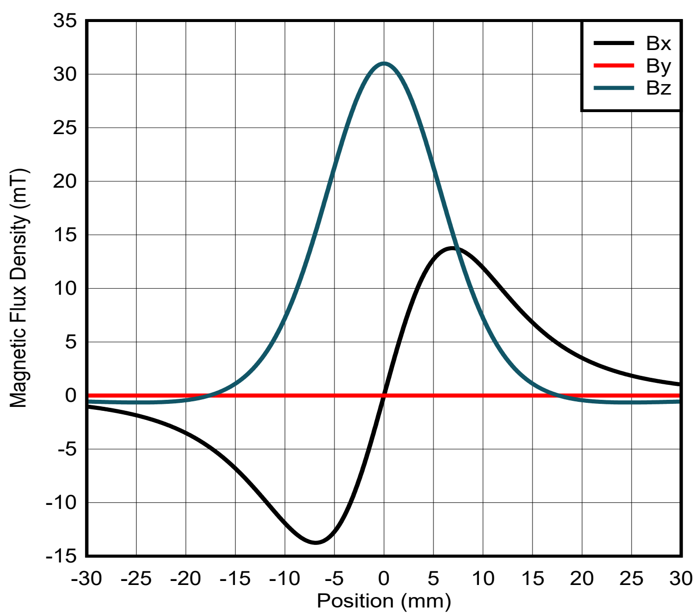

Figure 1-3. Example Magnetic Field Components Observed During Linear Motion

Examine how the selection of a magnet can impact the quality of the position measurement in a slide-by arrangement using a 3D sensor, and how to best linearize this measurement for minimal error.

2 Magnet Selection

Impact of Magnet Parameters

When selecting a magnet for a linear mover, consider temperature, magnetic material, magnet grade, magnet geometry, and general mechanical constraints. These system variables all have an impact on the overall function and reliability of the system.

As an example study, an axially magnetized cylinder magnet with a remanence (B_r) of 850 mT was simulated traveling above a sensor with an incrementally increased air gap.

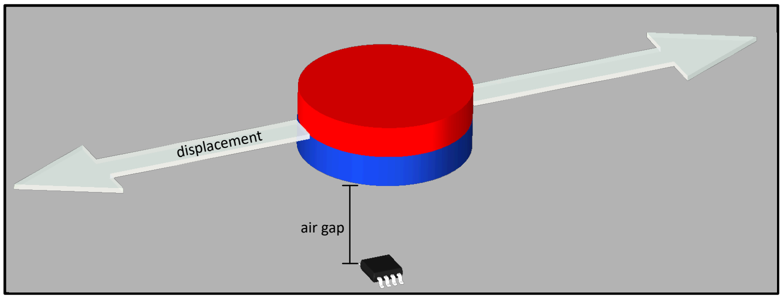

Figure 2-1. Slide-By Linear Magnetic Position Sensing

The magnet had an outer diameter of 16 mm and a thickness of 6 mm. Each horizontal line represents the magnitude of the vertical component (B_Z) of the observable magnetic flux density. Plotted together, a 3D heat map is produced that shows how this one field component varies in the region below the magnet. In this case, the horizontal displacement is swept from –40 mm to +40 mm, and the vertical air gap between the sensor and magnet ranges from 2 mm to 15 mm.

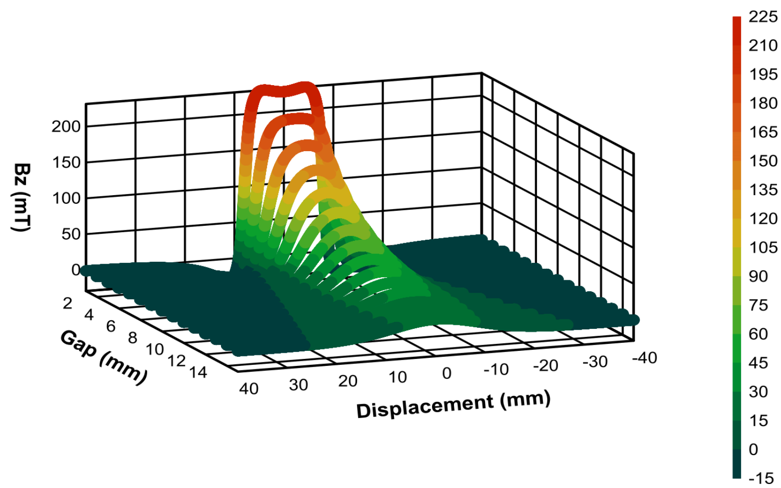

Figure 2-2. B-Field Z Component Versus Linear Position

In the case of TMAG5170, the device offers two variants, each with three user programmable input ranges that vary from ±25 mT to ±300 mT. Any inputs above the maximum range are not useful. Alternatively, the TMAG5170D-Q1 is a dual-die version of the TMAG5170 that can be used if redudency in the system is required.

When examining these results closely, when the air gap distance between the sensor element and magnet is very small, there is distortion near the peak of the bell-shaped input curve as the curve begins to flatten. At very close ranges, bad peaking results from the corner effects of the magnet body concentrating on the magnetic field.

For comparison, consider how a change in the magnet geometry can impact overall function. For instance, if the magnet had an outer diameter of 8 mm while all other parameters were the same, you can note several different changes in behavior.

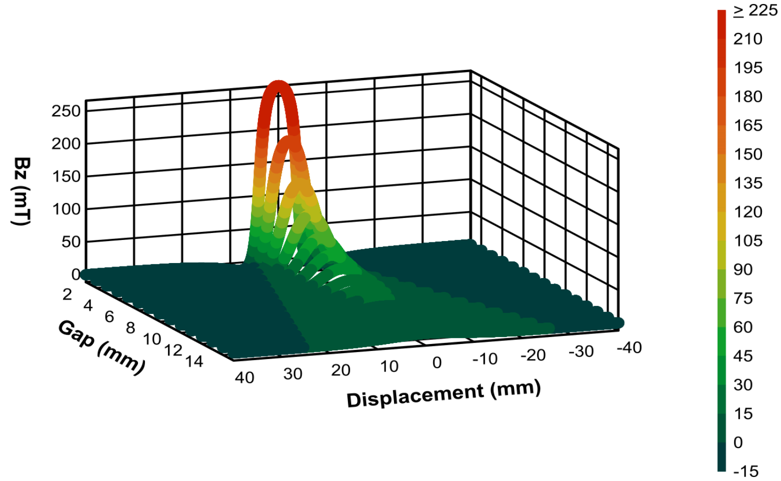

Figure 2-3. Linear Position Sweep With Reduced Magnet Diameter

One noted change is that the useful width of the input range dramatically reduced. The Calibration Method section explains that the maximum sensing range is typically at least 2x the diameter of the magnet.

Additionally, the corner effects observed at very close proximity are dramatically reduced when using a narrower magnet. The peak amplitude drops quickly when the air gap range increases. Intuitively, the sensing range for a smaller magnet is not as large as the sensing range of the original. What makes things even more difficult is that reducing the signal-to-noise ratio (SNR) increases uncertainty in any measurement. Therefore, target a peak input value nearly the full scale input range of the sensor selected.

Assuming then that the larger diameter is more desirable for the increased sensing range, another study of the impact of the magnet thickness can be informative. Consider next, the impact of increasing the thickness from 6 mm to 12 mm.

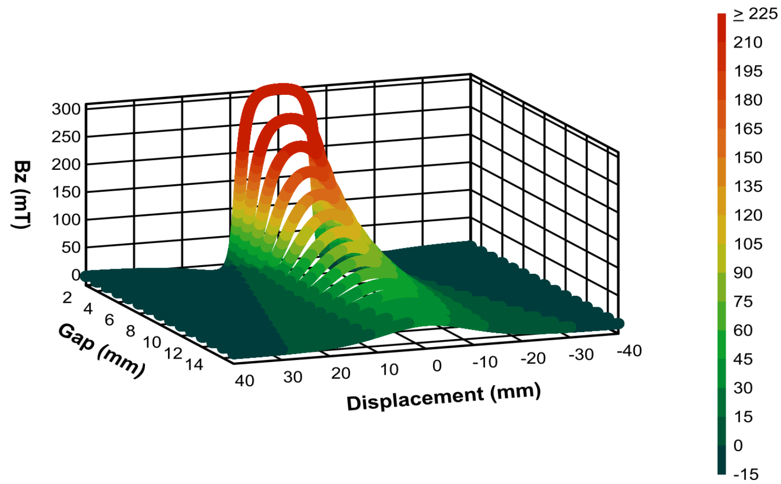

Figure 2-4. Linear Position Sweep With Increased Magnet Thickness

Similar to reducing the diameter of the magnet, increasing the thickness reduced the cornering effect, although visible distortion still occurs at very close proximity. From here, we can deduce that the ratio of the thickness to the diameter can impact the closest sensing range possible for this motion. Unsurprisingly, the peak B-field magnitude also increased when a magnet with larger mass was used.

Beyond just the considerations for magnet size, the material and grade of the magnet can impact field strength and cost to build the system. For example, magnetic materials can weaken as temperatures rise. Table 2-1 shows the typical values for this behavior.

Table 2-1. Magnetic Material Temperature Response

Material	Temperature Drift (C)
NdFeB	-0.12%/C
SmCo	-0.04%/C
AlNiCo	-0.02%/C
Ferrite	-0.2%/C

If the working environment experiences large temperature variations, consider selecting a Samarium Cobalt (SmCo) magnet to reduce the effects of temperature drift.

Consider the approximate working air gap range for the sensor. The magnetic flux density observed by the sensor is inversely proportional to the square of the distance. That is, as the range increases, expect to see exponential decay in the strength of the field.

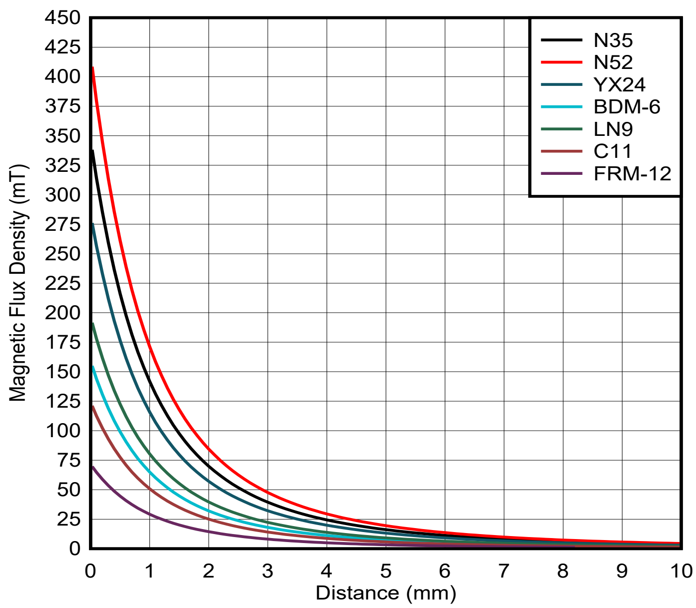

Figure 2-5. Magnetic Flux Density Versus Air Gap Range for Various Magnet Materials

For any magnetic material, there are often several different grades of magnets which are usually distinguished by the B_r of the material. This value is well defined for any particular material, regardless of the size of the magnet. As B_r decreases, the B-field for any specific shape magnet can weaken. Neodymium type magnets, such as N35 and N52, tend to be the strongest commercially available option and inexpensive ferrite materials such as FRM-12 tend to be the weakest.

Calibration Method

For any particular magnet selected, the position of the magnet can be calculated by deriving the mechanical angle using the arc-tangent of the outputs of the Hall-effect sensor.

For example, the input field produced by Figure 2-6 with a remanence of 850 mT is shown in the following plot.

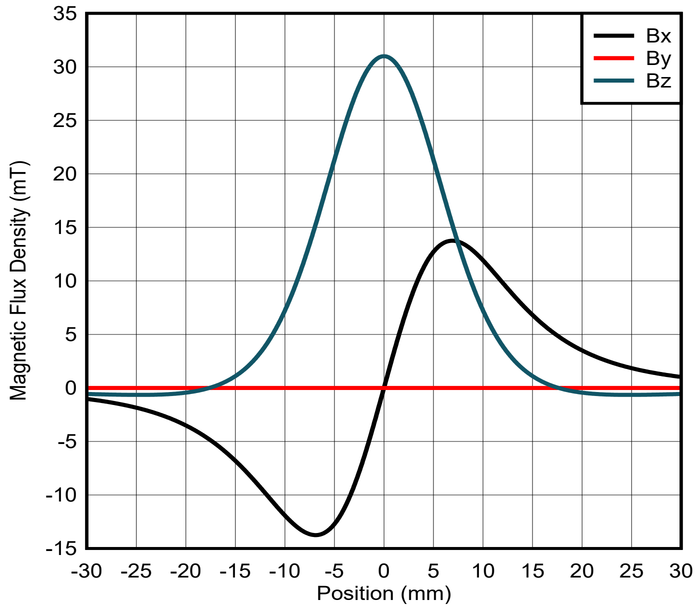

Figure 2-6. Magnet (10 mm ⌀ × 4 mm) at 10-mm Vertical Air Gap

Calculations of angle using these inputs directly can be compared to the real mechanical angle.

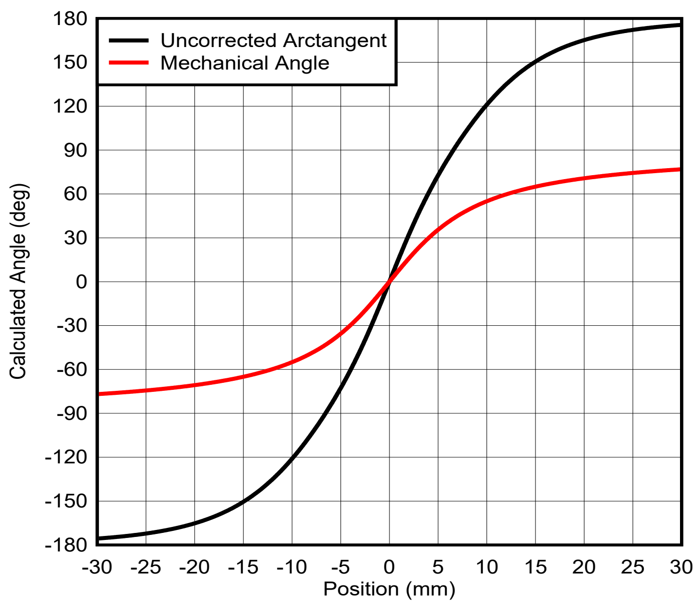

Figure 2-7. Mechanical Angle Versus Calculated Arctangent

Notice that the form is similar but is distorted somewhat in shape and extent. This distortion can be corrected using the following form:

$$Position = \tan\left(\gamma^{*}\operatorname{atan}\left(\frac{\alpha^{*}(B_Z - \beta)}{B_x}\right) + \varphi^{*}B_x\right)^{*}\frac{magnet\ thickness + airgap}{2} \quad (1)$$

In Equation 1, four specific correction factors are required to obtain linearity. **α** specifies the amplitude correction applied to the Z axis input, **β** specifies a fixed offset which must be applied to the Z axis input. **γ** is a scalar correction for the magnetic angle, and **φ** is a scalar factor of the Y axis input which corrects some non-linearity in the final result.

In this case, setting the following empirically derived values for each factor produce a final position accuracy shown in Figure 2-8.

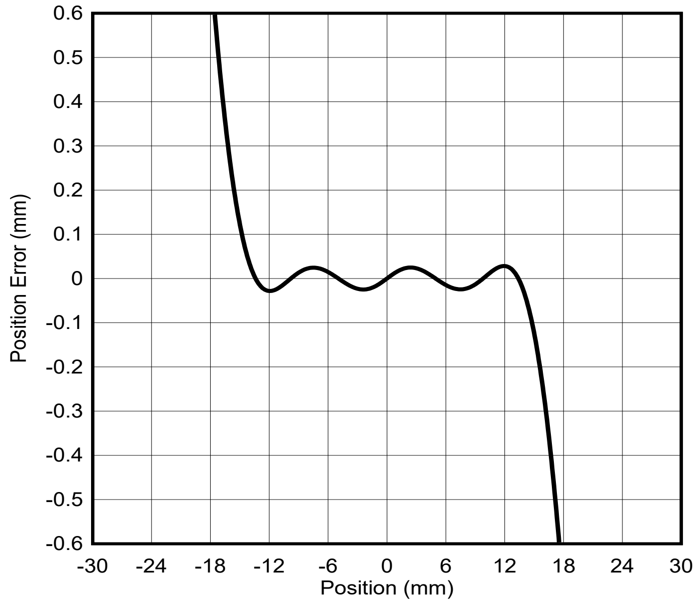

α = 0.791 ; **β** = 16.3 ; **γ** = 0.4104 ; **φ** = 0.448

Figure 2-8. Calibrated Position Error Versus Absolute Position

This same method was applied in the following figures to obtain similar accuracy. In each case, the position error is minimized over a region **approximately 2x the diameter** of the magnet.

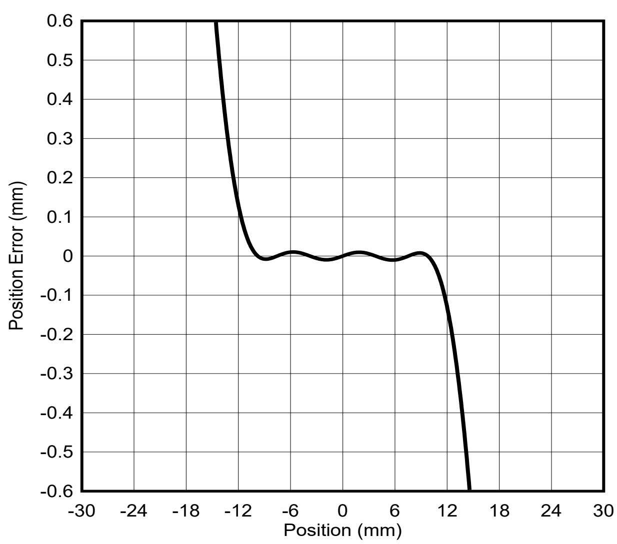

α = 0.833 ; **β** = 4.85 ; **γ** = 0.397 ; **φ** = 1.07

Figure 2-9. Position Error for Magnet (5 mm ⌀ × 4 mm) at 10-mm Air Gap

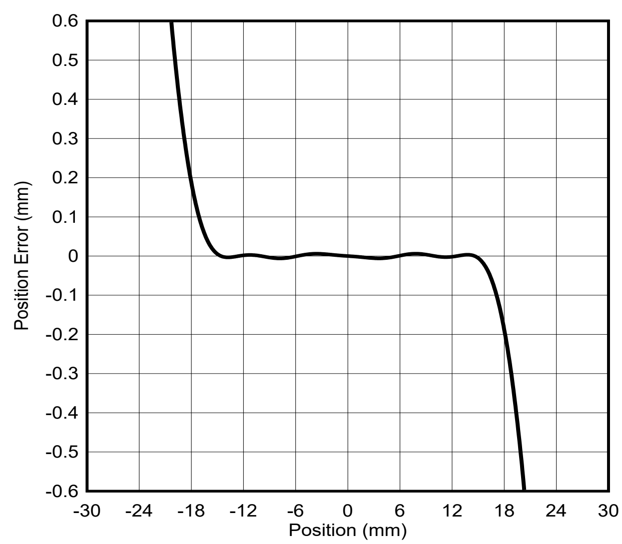

α = 0.739 ; **β** = 24.12 ; **γ** = 0.4215 ; **φ** = 0.4617

Figure 2-10. Position Error for Magnet (14 mm ⌀ × 4 mm) at 10-mm Air Gap

The quality of each calibration varies with the exactness of the correction factors applied. In the case of the largest diameter magnet, peak error in the sensing range is approximately 10 um.

Of similar note, the ratio of the potential sensing range to the magnet diameter is largest for the smaller (and weakest) magnet.

Similarly, varying the air gap distance is possible to demonstrate impact on the expected sensing range of the sensor. Consider the following plots based on the 14 mm ⌀ x 4 mm magnet at air gaps of 5 mm and 20 mm.

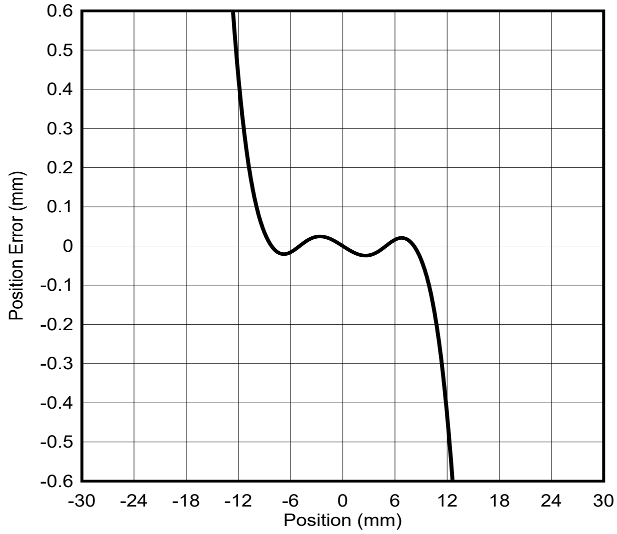

α = 0.79 ; β = 58.9 ; γ = 0.297 ; φ = 0.049

Figure 2-11. Position Error for Magnet (14 mm ⌀ × 4 mm) at 5-mm Air Gap

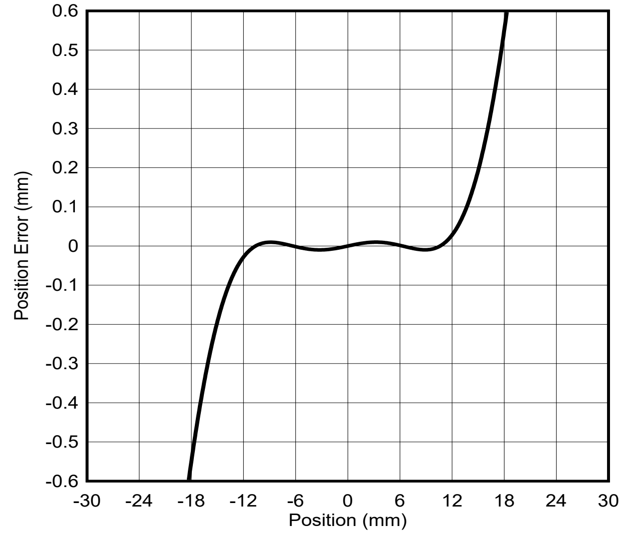

α = 0.775 ; β = 4.95 ; γ = 0.436 ; φ = 1.54

Figure 2-12. Position Error for Magnet (14 mm ⌀ × 4 mm) at 20-mm Air Gap

In both cases, the maximum sensing range for the magnet was reduced. In the case of the 5-mm air gap, the input field was limited by distortion. In the case of the 20-mm air gap, the sensing range is limited by the strength of the magnetic field. The design goal, therefore, is to target a strong magnetic field that neither saturates the input of the sensor nor becomes distorted due to close range of the magnet.

In some cases, using a bar-shaped magnet can be advantageous for ease of assembly. This calibration method is not limited to cylindrical magnets. Similar to the previous cases, implementing the same calibration method for a square-faced magnet traveling over the sensor can produce excellent linearity (see Figure 2-13).

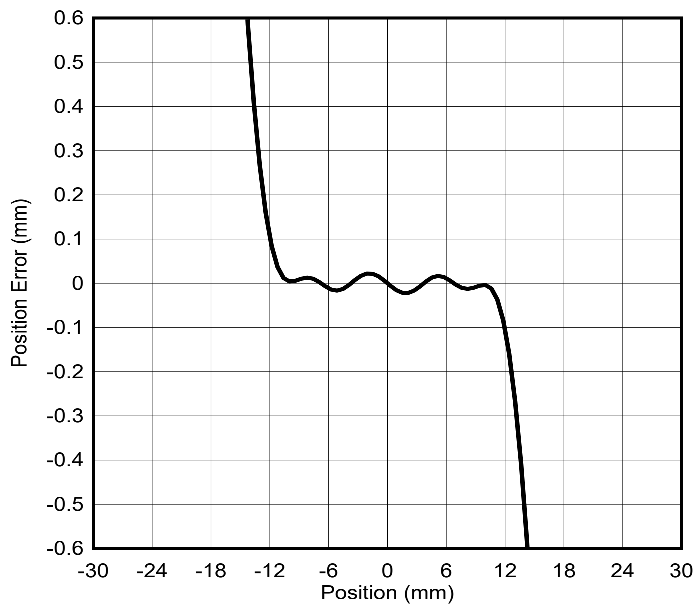

α = 0.75 ; β = 53.7 ; γ = 0.3815 ; φ = 0.089

Figure 2-13. Position Error for Magnet (10 mm × 10 mm × 4 mm) at 5-mm Air Gap

3 Summary

As was shown with the calibration results above, there are several options available to optimize the placement of each 3D Hall-effect sensor for long observable stroke distance. To get the highest quality results, a magnet which is strong enough to use most of the linear input range of the sensor is beneficial, and a wider magnet can produce a longer sensing range. In cases where air gap distance is minimized, use a thicker magnet to reduce distortion that can result near the corners of the magnet.

Implemented correctly, 3D Hall-effect sensors offer an increased sensing range by approximately 2x and as demonstrated in Figure 2-10 a linearity error of 10 µm is attainable. Maximizing the sensing range is critical to reducing the total number of sensors required in any linear position sensing application. Additionally, reducing linearity error is critical for precise control required for automated systems like linear motor transport systems to achieve quality and highly repeatable performance for manufacturing and assembly.

4 References

- Texas Instruments, *DRV5055 Ratiometric Linear Hall Effect Sensor*, data sheet.
- Texas Instruments, *Linear Hall-Effect Sensor Array Design*, application note.
- Texas Instruments, *TMAG5170 High-Precision 3D Linear Hall-Effect Sensor With SPI*, data sheet.
- Texas Instruments, *TMAG5273 Low-Power Linear 3D Hall-Effect Sensor With I2C Interface*, data sheet.

5 Revision History

Changes from Revision * (July 2022) to Revision A (May 2023)	Page
• Updated the numbering format for tables, figures, and cross-references throughout the document	1
• Added reference to TMAG5170D-Q1	4
• Added *References* section	11